DTU Library

Hardness loss and microstructure evolution of 90% hot-rolled pure tungsten at 1200-1350°C

Yu, Ming; Wang, Kang; Zan, Xiang; Pantleon, Wolfgang; Luo, Laima; Zhu, Xiaoyong; Wu, Yucheng

Link back to DTU Orbit

Hardness loss and microstructure evolution of 90% hot-rolled pure tungsten at 1200~1350℃

Ming Yu[1], Kang Wang[2], Xiang Zan*[1, 3, 5], Wolfgang Pantleon[4, 1], Laima Luo[1, 3, 5], Xiaoyong Zhu[3], Yucheng Wu*[1, 2, 3, 5]

[1] *School of Materials Science and Engineering, Hefei University of Technology, Hefei, Anhui, 230009, China*
[2] *Institute of Industry & Equipment Technology, Hefei University of Technology, Hefei, Anhui, 230009, China*
[3] *National–Local Joint Engineering Research Centre of Nonferrous Metals and Processing Technology, Hefei, Anhui, 230009, China*
[4] *Department of Mechanical Engineering, Technical University of Denmark, 2800 Kgs. Lyngby, Denmark*
[5] *Laboratory of Nonferrous Metal Material and Processing Engineering of Anhui Province, Hefei, Anhui, 230009, China*

Abstract: Tungsten is a promising plasma-facing material because of its low sputtering yield, high melting point and high thermal conductivity. The hardness loss and microstructure evolution of pure tungsten hot-rolled to 90% thickness reduction is investigated by isothermal annealing at temperature range of 1200 to 1350 °C. Changes in the mechanical properties caused by recovery and recrystallization during heat treatment are detected by Vickers hardness measurements. Additionally, the microstructural evolution is analyzed with light optical microscopy and X-ray diffraction. The results indicate that the hardness evolution can be divided into two stages: recovery and recrystallization. Recrystallization of W90 in the temperature range of 1200 to1350 °C is governed by the same activation energy as grain boundary diffusion. The average recrystallized grain size is larger for lower annealing temperatures.

Keywords: Tungsten; Recrystallization; Vickers hardness; Microscopy; X-ray diffraction

1. Introduction

Tungsten has potential applications in extremely challenging operation conditions, such as in plasma-facing components and helium-cooled divertors [1], which withstand both large energy load (10-15 MW/m^2) and temperature gradients [2, 3]. As a refractory metal, tungsten features several advantageous properties for fusion application, e.g. a high melting temperature of about 3695 K, good thermal conductivity, high creep resistance, good high-temperature strength and low vapor pressure [4, 5]. Tungsten has already been selected as a candidate material for ITER. Pure tungsten is generally manufactured through different technologies, including powder metallurgy [6, 7] and plastic deformation [8, 9]. Recovery, recrystallization and grain coarsening will occur in plastically deformed tungsten at high temperature. This will result in a loss of good properties (i.e., mechanical strength) and embrittlement[10, 11].

Even though many studies have been performed on pure tungsten, e.g., material design, mechanical behavior, high heat flux properties [12] and irradiation behavior [13, 14], there are only limited data available for recrystallization kinetics of rolled pure tungsten, e.g. [2, 15]. The present work investigates the recrystallization behavior of pure tungsten hot-rolled to 90% thickness reduction for four different annealing temperatures. The time periods required for half-recrystallization of pure tungsten at different annealing temperatures are determined; the recrystallization behavior is identified and described by established models.

2. Experiments

The material used in this study is commercially pure tungsten from Beijing Tianlong Tungsten Technology Co. Ltd. The as-received plates were hot-rolled to a thickness reduction of 90% (W90) at 1500 °C. Small specimens with a size of 6×7×8 mm^3 along normal direction (ND), transverse direction (TD) and rolling direction (RD) were cut from the plates by wire-cut electrical-discharge machining. The samples were placed individually in evacuated and sealed quartz tubes to avoid oxidation during heat treatment and subsequently isothermally annealed for various periods of time at four different temperatures within the range of 1200 to 1350 °C. The specimens (termed W90-1200, W90-1250, W90-1300 and W90-1350) were put into a pre-heated furnace, removed after the desired annealing time and cooled to room temperature by air-cooling.

For all samples, transversal sections (RD 8 mm × ND 6 mm) were investigated. The surface was prepared metallographically by subsequent mechanical grinding and polishing with silicon carbide paper, the final step with 800 grit paper. For light optical microscopy, the samples were etched with boiling 3 wt.% H_2O_2 solution [16]. Optical micrographs were obtained under polarized light to examine the evolution of the microstructure. Their texture was investigated by means of a X'Pert PRO MPD X-ray Diffractometer. Vickers hardness measurements were performed on the mechanically polished surfaces under a load of 0.2 kg and a dwell time of 10 s. The reported hardness values $HV_{0.2} \pm \Delta HV_{0.2}$ are averages over 10 indents with the standard deviation of the average $\Delta HV_{0.2}$; error bars in graphs represent $\pm \Delta HV_{0.2}$ as well.

---

* *Corresponding Author: Xiang Zan, Yucheng Wu*
     E-mail: zanx@hfut.edu.cn, ycwu@hfut.edu.cn

3. Results and discussion

3.1. Variation of Vickers hardness

Generally, the softening during an annealing treatment can be classified into three stages: recovery, recrystallization and grain coarsening. Recovery and grain coarsening lead to only minor changes in the hardness; therefore, the hardness loss due to recrystallization will be mainly investigated here. The progress of recrystallization is determined from the Vickers hardness ($HV_{0.2} \pm \Delta HV_{0.2}$) as function of annealing time. The evolution of the Vickers hardness during isothermal annealing at four different temperatures is illustrated in Fig. 1. From Fig. 1, it can be concluded that the hardness decreases monotonously from the value HV_{def} of the as-deformed state to the value HV_{rex} of the fully recrystallized state. The achieved steady stage after the initial drastic decrease in hardness indicates completion of recrystallization. Recrystallization is strongly influenced by the annealing temperature and the rate of recrystallization increases with the increased annealing temperature indicating a thermal activated process [17].
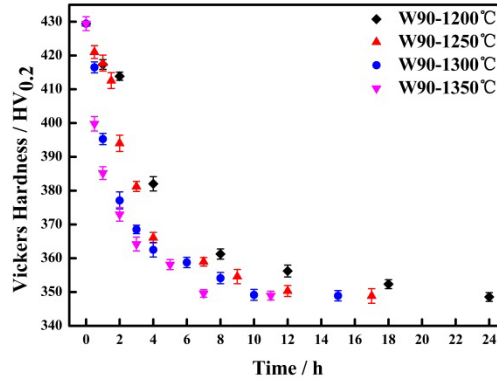

Fig. 1. Evolution of Vickers hardness of W90
during annealing at different temperatures

The isothermal annealing behavior of W90 as shown in Fig. 1 spans the first two softening stages, recovery and recrystallization. For the highest annealing temperature of 1350 °C, the time to the onset of recrystallization is extremely short; while for the lowest annealing temperature of 1200 °C, recrystallization initiates at about 2 h. Only before these incubation times, the effects of recovery could be assessed quantitatively, therefore, only the recrystallization stage will be discussed.

The experimentally determined hardness values are averages over recrystallized and non-recrystallized regions according to the rule of mixtures [15]:

$$HV = X \, HV_{rex} + (1 - X) HV_{rec} \qquad (1)$$

with the hardness of the recrystallized regions HV_{rex} and the hardness of the recovered matrix HV_{rec} weighted by their respective volume fractions X and $(1 - X)$, respectively. For the hardness of the recovered matrix, the hardness values measured at the onset of recrystallization (i.e. the incubation time in Table 1) are considered.

In this manner, the volume fraction of the recrystallized regions can be determined by

$$X = \frac{HV_{rec} - HV}{HV_{rec} - HV_{rex}} \qquad (2)$$

from the actual measured hardness value HV.

Recrystallization occurs by thermally activated nucleation and growth of new defect-free grains. The evolution of the recrystallized fraction follows the general Johnson–Mehl–Avrami–Kolmogorov (JMAK) kinetics [17]:

$$X = 1 - \exp(-b^n (t - t_{inc})^n) \qquad (3)$$

with a coefficient b describing thermal activation, the Avrami exponent n, and the incubation time t_{inc} before the onset of recrystallization. The incubation periods, during which only recovery occurs, depend strongly on the annealing temperature. They are taken as the times when onset of recrystallization becomes recognizable, highlighted in Fig. 3 and summarized in Table 1.

The evolution of the recrystallized volume fraction X is shown in Fig. 2. The symbols represent the experimental data obtained from hardness measurements by Eq. (2), the solid lines being the description achieved by fitting the JMAK model (Eq. (3)). Combining Eqs. (1) to (3), the evolution of the Vickers hardness can be described as shown in Fig. 3. The values of b and n shown in Table 1 are obtained by non-linear fitting.
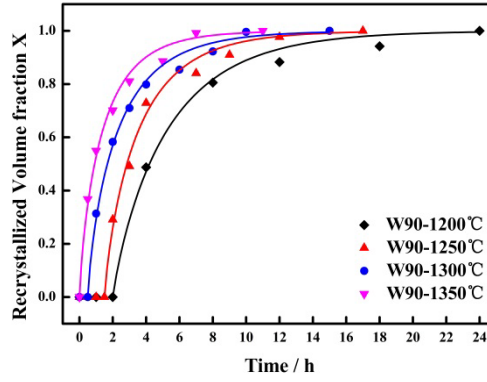
Fig. 2. Evolution of recrystallized volume fraction X of W90 during annealing at different temperatures.
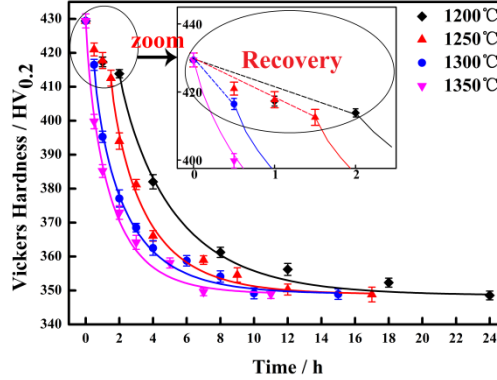

Fig. 3. Evolution of Vickers hardness of W90 during annealing at different temperatures. The lines represent the obtained fits by Eqs. (1) and (2). The insert highlights the hardness loss occurring during recovery before any onset of recrystallization.

Table 1 Values of the different parameters describing the recrystallization kinetics of W90. b and n are obtained as best fits of JMAK kinetics, t_{inc} as onset of recrystallization.

T (°C)	b (h^{-1})	n	t_{inc}(h)
1200	0.30	0.90	2
1250	0.48	0.84	1.5
1300	0.54	0.81	0.5
1350	0.70	0.81	0

The exponent n is rather constant within a range of 0.81-0.90 for the all investigated annealing temperatures. As the annealing temperature increases, the value of b increases accordingly reflecting the thermal activation of the process.

The time to half-recrystallization ($t_{x=0.5}$), obtained from Eq. (3), depends on annealing temperature T according to an Arrhenius relationship:

$$t_{x=0.5} = t_0 \exp(E_{t_{X=0.5}}/RT) \qquad (4)$$

with a constant t_0, the universal gas constant R and the apparent activation energy $E_{t_{x=0.5}}$ for half-recrystallization. In the corresponding Arrhenius plot in Fig. 4, i.e. a plot of $\ln t_{x=0.5}$ against 1/T, a straight line is expected. Accordingly, the apparent activation energy for half-recrystallization of the 90% hot-rolled plates is 203 kJ/mol. This activation energy is comparable to findings of the activation of grain boundary diffusion as 210.7 kJ/mol [18] (at 1500-1900 °C) and 294 kJ/mol [19] (at 887-1050 °C): It should be mentioned that other sources [20] quantify the activation energy for grain boundary diffusion to be 377-460 kJ/mol.
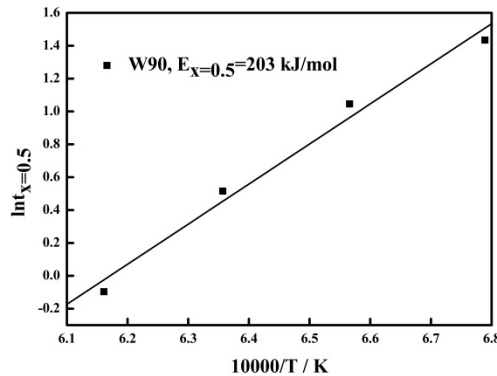

Fig. 4. Arrhenius plot of the dependence of the time to half -recrystallization in W90 on annealing temperature

3.2. Microstructural evolution

The microstructure in the RD/ND section of the as-deformed state, several partially recrystallized states and the fully recrystallized states are shown in Fig. 5 to illustrate the effect of the annealing temperature on recrystallization of W90. In all cases, the micrographs were stitched form 6 individual images to obtain a larger field of view of 0.618 × 0.464 mm². The micrographs clearly show that the deformation structure of the as-received state after hot-rolling with elongated grains along the rolling direction (RD) becomes gradually replaced by equiaxed recrystallized grains. After several hours of annealing, a fully recrystallized structure with equiaxed grains is achieved.

For the fully recrystallized states, grain boundaries were delineated and individual recrystallized grains identified by Adobe Photoshop and IPP software. The resulting boundary maps of W90 fully recrystallized at three different annealing temperatures are shown in Fig. 6.

For quantifying the grain size, the equivalent circular diameter (ECD)

$$D = 2\sqrt{\frac{A}{\pi}} \qquad (5)$$

which represents the diameter of a circular disc with the same area as the apparent grain area A determined by IPP, because of the different and irregular shapes of the grains in the boundary maps.
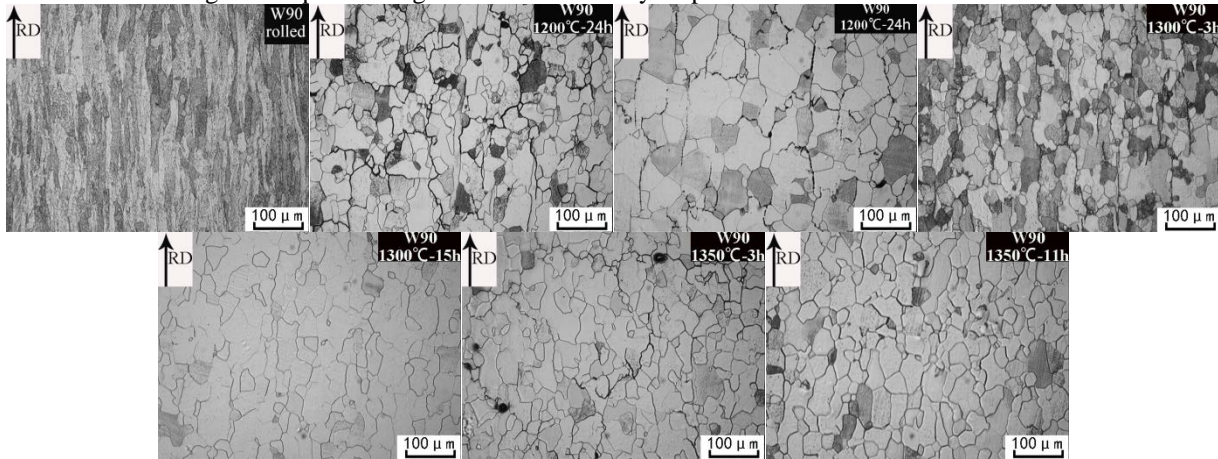

Fig. 5. Microstructure of tungsten hot-rolled to 90% thickness reduction after annealing at different temperatures.
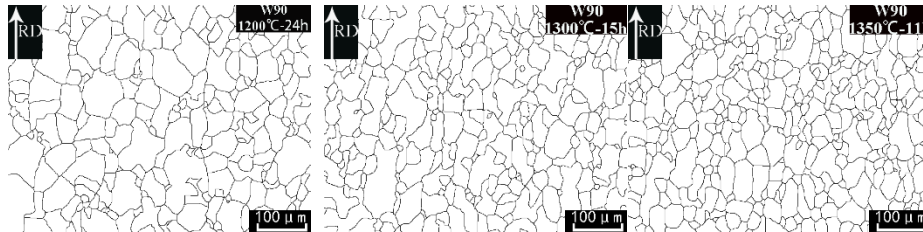

Fig. 6. Digitized images of W90 with after full recrystallization at different temperatures.

The grain size distributions for fully recrystallized W90 after annealing at three different temperatures are shown in Fig. 7. The average grain size was determined as area weighted average of the ECD over the entire region. This average ECDs were 28 μm, 32 μm and 35 μm for the fully recrystallized W90 annealed at 1350 °C, 1300 °C and 1200 °C, respectively. Obviously, the average recrystallized grain size becomes larger at lower annealing temperature, which can also be seen from Fig. 5 and Fig. 6. Such a smaller grain size at higher annealing temperature could be the result of an increased nuclei density at higher temperatures, while at lower temperatures less nuclei might be formed [21].
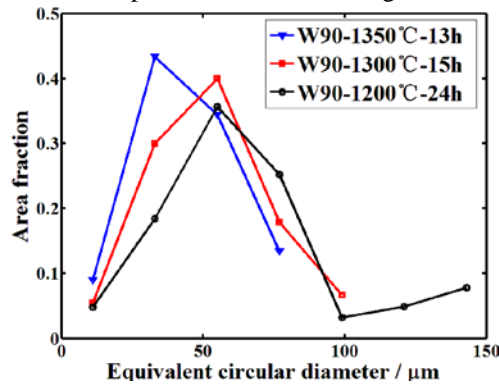

Fig. 7. Grain size distribution of fully recrystallized W90 achieved by isothermally annealing at different temperatures for different times.

X-ray diffraction was performed on the ND/RD surface of the as-received and two annealed conditions for all test temperatures. Fig. 8 shows the measured diffractograms of W90-1200、W90-1250、W90-1300 and W90-1350 which indicate subtle changes during the annealing process. Obviously, the highest diffraction intensity is always (110) peak as expected from the theoretical intensities; all measured intensities in the as-received state follow generally the expectations for a random texture (see table 2).
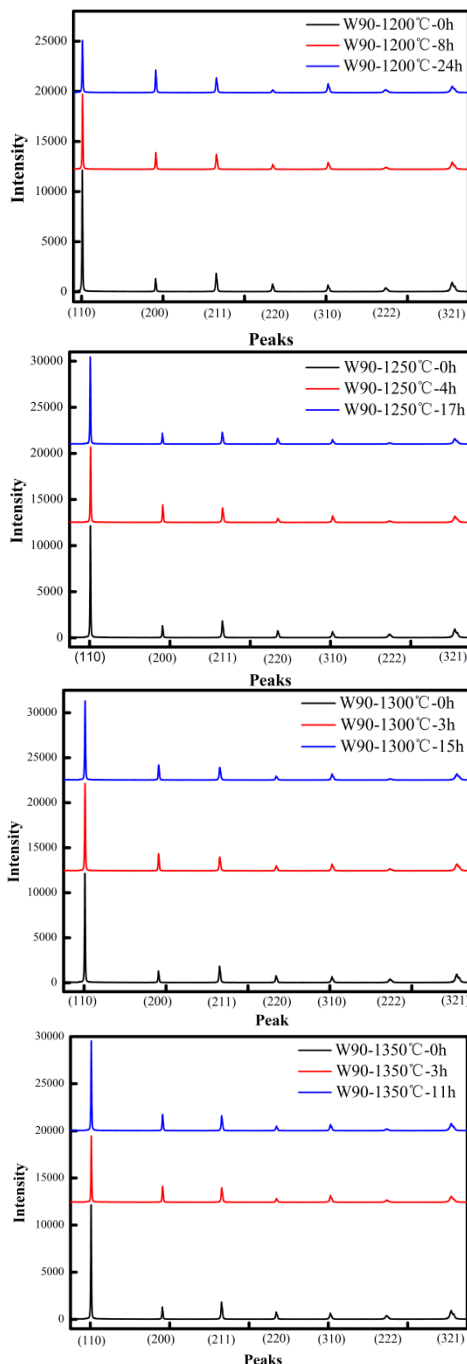

Fig. 8 Diffractograms of W90 annealed at different temperatures. The horizontal axes represent diffraction angles 2θ from 30° to 135°. The indizes of the expected peaks are indicated.

In order to highlight the differences between the diffractograms, the integrated intensity of each recorded peak was determined by integrating the intensity over an interval of 3° in 2θ after subtracting the background. Further information about the texture can be gained by normalizing the relative intensities by the intensity of the 110 peak as shown in Table 2. In order to quantify the ratio between different texture components, the ratio between the sum of the integrated intensities of the (110) and (220) reflections and the total intensity of all reflections is calculated and given in the table as (110)+(220)/all. This ratio assumes approximately the value for a random texture in the as-received state and decreases significantly during annealing, in particular for annealing at 1200 °C, indicating the formation of a recrystallization texture.

Table 2. The integrated intensity of X - ray diffraction peaks as measured on the RD/ND surface of tungsten hot-rolled to 90% thickness reduction after isothermal annealing. For comparison purposes, the expected intensity rations according to JSPDS card 04-0806 for tungsten are added.

Annealing		(110)	(200)	(211)	(220)	(310)	(222)	(321)	(110)+(220)/all
1200 °C	0h	100	13.2	25.6	12.0	11.5	10.2	29.0	0.56
	8h	100	29.2	34.6	12.3	20.3	8.8	35.4	0.47
	24h	100	50.7	44.1	9.9	34.3	19.0	42.8	0.37
1250 °C	0h	100	13.2	25.6	12.0	11.5	10.2	29.0	0.56
	4h	100	28.6	31.9	10.4	18.5	6.8	30.7	0.49
	17h	100	14.2	22.9	11.9	10.9	4.0	24.1	0.60
1300 °C	0h	100	13.2	25.6	12.0	11.5	10.2	29.0	0.56
	3h	100	24.3	26.8	11.0	16.9	7.33	30.2	0.51
	15h	100	24.4	27.4	9.94	17.2	4.89	28.9	0.52
1350 °C	0h	100	13.2	25.6	12.0	11.5	10.2	29.0	0.56
	3h	100	31.8	38.0	10.9	24.1	10.7	35.6	0.44
	11h	100	23.1	27.4	9.76	15.4	6.16	29.8	0.52
JCPDS		100	15	23	8	11	4	18	0.61

4. Conclusions

The recrystallization behavior of pure tungsten subjected to 90% thickness reduction by hot-rolling is investigated by means of Vickers hardness testing, light optical microscopy and X-ray diffraction. The hardness loss during the recrystallization can be nicely fitted by the Johnson-Mehl-Avrami-Kolmogorov kinetics, if an incubation time is taken into consideration. The apparent activation energy for half-recrystallization of W90 is found as 203 kJ/mol similar to the activation energy of grain boundary diffusion. During heat treatment, elongated grains along the rolling direction in the deformation structure become gradually replaced by equiaxed recrystallized grains. The average recrystallized grain size is larger for lower annealing temperature as higher recrystallization temperatures may cause an increased probability to form nuclei.

Acknowledgements

References

[1] Rieth, M., Dudarev, S.L., Gonzalez de Vicente, S.M., et al., Recent progress in research on tungsten materials for nuclear fusion applications in Europe, Journal of Nuclear Materials. 432 (2013) 482-500.

[2] Alfonso, A., Juul Jensen, D., Luo, G.N., et al., Recrystallization kinetics of warm-rolled tungsten in the temperature range 1150–1350 °C, Journal of Nuclear Materials. 455 (2014) 591-594.

[3] Pintsuk, G., Prokhodtseva, A. and Uytdenhouwen, I., Thermal shock characterization of tungsten deformed in two orthogonal directions, Journal of Nuclear Materials. 417 (2011) 481-486.

[4] Wirtz, M., Linke, J., Pintsuk, G., et al., Thermal shock behaviour of tungsten after high flux H-plasma loading, Journal of Nuclear Materials. 443 (2013) 497-501.

[5] Wurster, S., Baluc, N., Battabyal, M., et al., Recent progress in R&D on tungsten alloys for divertor structural and plasma facing materials, Journal of Nuclear Materials. 442 (2013) S181-S189.

[6] Piotter, V., Zeep, B., Norajitra, P., et al., Development of a powder metallurgy process for tungsten components, Fusion Engineering and Design. 83 (2008) 1517-1520.

[7] Wang, J., Zhao, G., Chen, L., et al., A comparative study of several constitutive models for powder metallurgy tungsten at elevated temperature, Materials & Design. 90 (2016) 91-100.

[8] Wei, Q., Zhang, H.T., Schuster, B.E., et al., Microstructure and mechanical properties of super-strong nanocrystalline tungsten processed by high-pressure torsion, Acta Materialia. 54 (2006) 4079-4089.

[9] Chen, Z., Han, W., Yu, J., et al., Microstructure and helium irradiation performance of high purity tungsten processed by cold rolling, Journal of Nuclear Materials. 479 (2016) 418-425.

[10] Babak, A.V. and Uskov, E.I., High-temperature embrittlement of tungsten, Strength of Materials. 15 (1983) 667-672.

[11] Mathaudhu, S.N., deRosset, A.J., Hartwig, K.T., et al., Microstructures and recrystallization behavior of severely hot-deformed tungsten, Materials Science and Engineering: A. 503 (2009) 28-31.

[12] Liu, X., Tamura, S., Tokunaga, K., et al., High heat flux properties of pure tungsten and plasma sprayed tungsten coatings, Journal of Nuclear Materials. 329–333, Part A (2004) 687-691.

[13] Watanabe, H., Futagami, N., Naitou, S., et al., Microstructure and thermal desorption of deuterium in heavy-ion-irradiated pure tungsten, Journal of Nuclear Materials. 455 (2014) 51-55.

[14] Zhang, Z.X., Chen, D.S., Han, W.T., et al., Irradiation hardening in pure tungsten before and after recrystallization, Fusion Engineering and Design. 98–99 (2015) 2103-2107.

[15] Alfonso, A., Juul Jensen, D., Luo, G.N., et al., Thermal stability of a highly-deformed warm-rolled tungsten plate in the temperature range 1100–1250 °C, Fusion Engineering and Design. 98–99 (2015) 1924-1928.

[16] Petzow, G., Metallographic etching : techniques for metallography, ceramography, plastography, ASM International, 1999.

[17] Humphreys, F.J. and Hatherly, M., *Recrystallization and related annealing phenomena (Second Edition)*. 2004, Pergamon: Oxford.

[18] Almanstötter, J. and Rühle, M., Grain growth phenomena in tungsten wire, International Journal of Refractory Metals & Hard Materials. 15 (1997) 295-300.

[19] Lee, J.S., Minkwitz, C. and Herzig, C., Grain Boundary Self-Diffusion in Polycrystalline Tungsten at Low Temperatures, physica status solidi (b). 202 (1997) 931-940.

[20] Lassner, E. and Schubert, W.D., Tungsten: properties, chemistry, technology of the element, alloys, and chemical compounds, Springers, Springers US: Boston, MA, 1999.

[21] Raabe, D., *Recovery and recrystallization: phenomena, physics, models, simulation*, in *Physical Metallurgy (Fifth Edition)*, K. Hono, Editor. 2014, Elsevier: Oxford. p. 2291-2397.